Amino-functionalized dendritic mesoporous silica nanoparticles for removal of copper from aqueous solutions

Junjie Yu[1], Antonina Bondarieva[1*], Ihor Pylypenko[1], Viktoriia Tobilko[1],
Tomash Sabov[2], Mariana Gumenna[3], Tamara Tomila[4], Olena Inshyna[5]

1 Department of Chemical Technology of Ceramics and Glass, National Technical University of Ukraine "Igor Sikorsky Kyiv Polytechnic Institute", 37 Beresteiskyi Ave., 03056, Kyiv, Ukraine
2 V. Ye. Lashkaryov Institute of Semiconductor Physics of NAS of Ukraine, 45 Nauky Ave., 03028, Kyiv, Ukraine
3 Department of Chemistry of Oligomers and Network Polymers, Institute of Macromolecular Chemistry of NAS of Ukraine, 48 Kharkivske Sh., 02155, Kyiv, Ukraine
4 Department of Physical Chemistry and Technology of Nanostructural Ceramics and Nanocomposites, Frantsevich Institute for Problems of Materials Science of NAS of Ukraine, 3 Omeliana Pritsaka Str., 03142, Kyiv, Ukraine
5 Department of Heterogeneous Acid-Base Catalysis, Institute for Sorption and Problems of Endoecology of NAS of Ukraine, 13 General Naumov Str., 03164 Kyiv, Ukraine
* Corresponding author's e-mail: a.i.bondarieva@gmail.com

ABSTRACT

The amino functionalisation of the surface of dendritic mesoporous silica nanoparticles (DMSN) was carried out via post-coupling using 3-Aminopropyltriethoxysilane (APTES) in an aqueous-alcohol medium. The physico-chemical characteristics of the synthesised material were studied using Fourier-transform infrared spectroscopy (FTIR), low-temperature nitrogen adsorption/desorption, differential thermal analysis (DTA), thermogravimetric analysis (TGA), and X-ray photoelectron spectroscopy (XPS). The quantity of specific functional groups presents on the DMSN surface before (-OH group) and after (-NH$_2$ group) functionalisation was determined by means of titration. The adsorption capacity of the materials for copper ions was investigated in the concentration range of 10 to 100 mg/L. Additionally, the effects of the pH of the aqueous medium and the contact time between the potential adsorbent and the contaminated solution on Cu(II) removal efficiency were examined. The equilibrium copper concentration was determined using inductively coupled plasma atomic emission spectroscopy (ICP-OES). It was found that surface modification of DMSN led to a more than tenfold increase in the number of functional groups and corresponding adsorption centres. As a result, the efficiency of copper ion removal within the pH range of 3–6 increased to over 87%. The adsorption equilibrium time decreased from 60 to 15 minutes. The maximum adsorption capacity for the amine-functionalised sample reached 35 mg/g, compared to just 0.62 mg/g for the unmodified DMSN. Pseudo-first-order and pseudo-second-order kinetic models, along with Langmuir and Freundlich isotherm models, were applied to analyse the adsorption mechanism. XPS analysis of the spent adsorbent further supported assumptions regarding the copper ion adsorption process.

Keywords: silica, 3-Aminopropyltriethoxysilane, surface, modification, adsorption, water treatment.

INTRODUCTION

Environmental pollution by heavy metals is becoming an increasingly serious problem, raising significant concern due to its negative effects on natural ecosystems and human health (Vareda et al., 2019). Unlike organic pollutants, heavy metals are not naturally biodegradable and can accumulate at all levels of the food chain, leading to toxic and carcinogenic concentrations (Adriano et al., 2004).

The list of such heavy metals includes copper, which enters aquatic environments primarily through wastewater from electroplating (Lejwoda et al., 2023) and metallurgical (Izydorczyk et al., 2021) industries, as well as from the production and

use of pesticides (Mohajerani et al., 2018; Husak, 2015), fertilizers (Shaw et al., 2020), and anti-fouling paints used as coatings for ship hulls, buoys, and underwater surfaces (Lagerström et al., 2020). Improper waste disposal and other anthropogenic activities also contribute to copper contamination.

Various conventional methods are employed to remove excess copper ions from water and maintain concentrations below the maximum permissible levels (WHO recommended safe limit in wastewater: 1 mg/L; United States Environmental Protection Agency: 1.3 mg/L). These methods range from chemical precipitation to electrodialysis and photocatalysis (Shrestha et al., 2021; Saravanan et al., 2021).

The choice of a specific treatment method depends on factors such as the initial Cu(II) concentration, the chemical composition and pH of the water, regulatory standards for treated water, and available technical resources. As a result, different processes are often combined to achieve the desired water quality in the most cost-effective manner (Ko, 2024; Azimi et al., 2017).

At the final stages of water purification and treatment, adsorption methods are recommended to achieve the lowest residual concentrations of inorganic toxicants. This is due to their relatively low operating costs, ease of implementation, and the availability of a wide range of adsorbent materials of inorganic (Zito et al., 2015; Kovalchuk et al., 2023), organic (Hao et al., 2023; Rasheed et al., 2020), biological (Anastopoulos et al., 2017; Solangi et al., 2021), and combined origins (Gil et al., 2021; Crini et al., 2018; Hokkanen et al., 2016).

Additionally, the desorption process can produce a concentrated stream of Cu(II), enabling the potential recovery of this heavy metal, which aligns with the principles of the circular economy and sustainable development strategies.

A review of scientific studies from the past decade indicates that traditional adsorbents such as clay minerals, activated carbon, and ion exchange resins exhibit a high capacity for heavy metal ion adsorption (Uddin, 2017; Zhang et al., 2021; Kołodyńska et al., 2017; Nekouei et al., 2019). However, due to their limitations, including restricted selectivity and adsorption capacity, extensive research is ongoing to develop new materials with enhanced properties.

Activation of the adsorbent surface with functional groups such as -SH, -NH$_2$, and -COOH is one of the most promising approaches for enhancing affinity toward target heavy metal ions.

Additionally, many researchers combine these functional groups (-SH, -NH$_2$, and -COOH) with heteroatoms (O, N, S) in clay minerals to further improve adsorption performance (Tan et al., 2020).

Amino groups (-NH$_2$) are particularly effective for removing heavy metal cations from aqueous media. Due to their lone electron pair and ability to act as Lewis bases, they readily form coordinate bonds with heavy metal ions (Lewis acids). In most cases, amino silanes are used as modifiers for the grafting of amino groups onto various substrates (Wamba et al., 2018; Kostenko et al., 2019).

This approach can be applied to a wide range of materials, including aerosil, silica, silica gel, clay minerals, and even biosorbents (Arce et al., 2015; Najafi et al., 2012; Yang et al., 2020). For example, studies have demonstrated that functionalizing zeolite from the Tsagaan-Tsav deposit (Mongolia) with 3-aminopropyltriethoxysilane (APTES) significantly enhances Cu(II) ion removal from contaminated water (Shirendev et al., 2022).

Dendritic mesoporous silica nanoparticles (DMSN) are particularly attractive adsorbents due to their high specific surface area, uniform pore and particle size, chemical stability, and excellent surface functionalization capability (Xu et al., 2022). Their unique dendritic-fiber morphology ensures that adsorption sites are easily accessible from all directions, further improving their efficiency in metal ion removal.

The papers (Cabañas et al., 2018; Estevão et al., 2021) demonstrate the potential for functionalizing mesoporous silica nanoparticles via the co-condensation method using amino organosilane for biomedical applications. In another study, Marconi et al. (2023) post-grafted amino groups onto dendritic fibrous mesoporous silica nanoparticles for the controlled release of corrosion inhibitors. Additionally, Otalvaro et al. (2019) reported successful selective adsorption of antibiotics and dyes using amino-functionalized mesoporous silica as an adsorbent material.

Other structurally distinct silica materials modified with APTES have also shown promising results in removing various cationic heavy metals from contaminated aqueous solutions (Dhaffouli et al., 2024; Ramasamy et al., 2017). However, there are relatively few studies focused specifically on copper adsorption. For example, Kuśmierek et al. (2025) investigated the potential of hydrophilic commercial silica functionalized with APTES for the adsorption of copper ions from aqueous solutions.

Therefore, the development of DMSN-based materials with enhanced affinity for copper cations and potentially other heavy metals or gases through surface functionalization using APTES presents an intriguing research direction, which is the focus of this study.

MATERIALS AND METHODS

Materials

Chemical and reagents

Cetyltrimethylammonium bromide (CTAB), sodium salicylate (NaSal), tetraethoxysilane (TEOS), triethanolamine (TEA), and copper(II) sulfate pentahydrate ($CuSO_4 \cdot 5H_2O$) were used in this study and were purchased from Merck. 3-Aminopropyltriethoxysilane (APTES) was obrained from Sigma-Aldrich, while sodium hydroxide (NaOH) was sourced from Ineos Group (France), and sodium chloride (NaCl) from Brenntag SE (Germany). Distilled water and ethanol (EtOH) were used as solvents. All chemicals were of analytical grade and used without further purification.

Synthesis of functionalized silica nanoparticles

The synthesis of DMSN was carried out by alkaline hydrolysis in an aqueous-alcohol solution using structure-forming agents, namely cetyltrimethylammonium bromide (CTAB) and sodium salicylate (NaSal), in combination with an inorganic precursor, namely tetraethoxysilane (TEOS), according to the method described by Yu et al., 2024. The duration of the synthesis was 1.5 hours at a temperature of 80 °C.

The amino functionalization of the surface of the synthesized DMSN was carried out by post-coupling using 3-Aminopropyltriethoxysilane (APTES) in an aqueous-alcoholic medium according to a modified procedure described by Tobilko et al., 2019. For this purpose, a DMSN sample was placed in a water-alcohol solution (1:3) acidified with concentrated HCl. The mixture was transferred to a three-necked flask in a thermostat maintained temperature 80 °C. With constant stirring, the APTES alcohol solution was added dropwise to the system using a peristaltic pump over the course of 1 hour. Figure 1 shows a schematic of the setup illustrating this process.

After that, the mixture was left in a drying oven at 80 °C for an additional 10 hours to complete the reaction. The resulting product was repeatedly washed with ethanol until a neutral pH value was achieved. The solid phase was separated from the liquid phase by centrifugation and dried at 60 °C.

Methods

Characterization of materials

The Fourier-transform infrared spectroscopy (FTIR) study was carried out in the wavelength range of 4000–400 cm^{-1} using a Fourier spectrometer FSM 1201 with the standard method of tableting with potassium bromide (KBr). The samples under study were thoroughly mixed with KBr powder in a mass ratio of 1:300, and the resulting mixture was pressed into transparent tablets with a diameter of 13 mm.

Low-temperature nitrogen adsorption/desorption was performed on the pre-evacuated samples using a Quantachrome NOVA-2200e Surface Area and Pore Size Analyzer. Data processing was carried out using the ASiQwin software. The specific surface area (S_{BET}, m^2/g) was calculated by
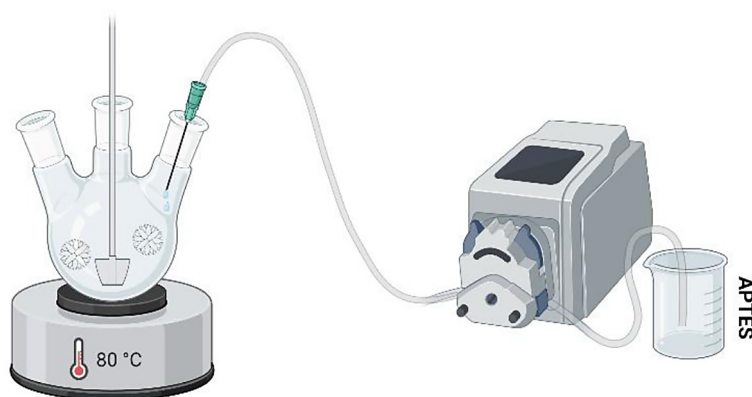

Figure 1. Schematic diagram of the installation for amino functionalization of DMSN surface

the multipoint BET method (Brunauer, Emmett and Teller). The total pore volume (V_Σ, cm³/g) was determined using the maximum adsorbed volume of nitrogen at a relative pressure $p/p_o \approx 1$. The pore size distribution was measured using by the BJH (Barrett-Joyner-Halenda) model. The average pore radius (R, nm) was calculated using the Equation 1:

$$R = \frac{2V_\Sigma}{S_{BET}} \qquad (1)$$

where: V_Σ – total pore volume, cm³/g; S_{BET} – specific surface area, m²/g.

Differential thermal and thermogravimetric analysis (DTA/TG) was performed on a derivatograph (Q-1000, MOM) in the temperature range from 20 °C to 1000 °C, with heating in air a rate of 5 °C/min. Al_2O_3 was used as a comparison sample.

The X-ray photoelectron spectroscopy (XPS) analyses were carried out with a PHI 5600 spectrometer using a monochromatic Al K(alpha) source. The instrument work function was calibrated to give a binding energy (BE) of 84 eV for the Au $4f_{7/2}$ line of metallic gold, and the spectrometer dispersion was adjusted to give a BE of 932.6 eV for the Cu $2p_{3/2}$ line of metallic copper. Survey scan analyses were carried out with a pass energy of 93.9 eV and a step size of 0.2 eV. The charge neutralization on the samples was adjusted to get the peak position of C 1s C-C peak at 284.8 eV.

Determination of the content of functional groups

The method of reverse titration of benzoic acid in 0.05 N toluene with KOH solution in the presence of bromothymol blue indicator was used to determine the total concentration of the main centers [B] (Tanabe et al., 1990). A 100 mg sample of DMSN, pre-annealed and cooled to room temperature without exposure to moisture, was added with 10 ml of a 0.05 N solution of benzoic acid in toluene. After 30 minutes of stirring, a 3 ml aliquot of the sample was taken and titrated. The amount of adsorbed benzoic acid was calculated from the difference between the amount of acid taken and the amount determined after adsorption.

The content of amino (-NH₂) groups (meq/g) was determined by the acid-base back-titration method (Moaseri et al., 2013). The weighted DMSN-NH₂ sample (at least 100 mg) was immersed in 20 ml HCl (0.1 N) for 24 h, and the resulting solution was titrated with KOH (0.1 N).

The content of -NH₂ groups was calculated by the following Equation 2:

$$The\ content\ of\ NH_2\ groups =$$
$$= \frac{V_{HCl}N_{HCl} - V_{KOH}N_{KOH}}{m} \qquad (2)$$

where: V is the volume of acid and alkali taken for titration, ml; N is the equivalent concentration of acid and alkali taken for titration, N; m is the mass of the sample, g.

Adsorption experiments

The adsorption capacity of the obtained samples was evaluated using model solutions contaminated with Cu(II) ions in the concentration range of 10–100 mg/L. The ionic strength (I = 0.01) was adjusted with a 1 M NaCl solution. The pH value was adjusted with 0.1 M NaOH solution and controlled with a pH meter (ADWA AD1020).

Experimental studies of the effect of pH on the degree of purification of model solutions from Cu(II) ions were carried out in the pH range from 3 to 6, which corresponds to the range of pH values with the highest percentage of Cu^{2+} form. The removal efficiency (R, %) of copper (II) ions was estimated by Equation 3:

$$R = \frac{C_{in} - C_{eq}}{C_{in}} \cdot 100\% \qquad (3)$$

where: C_{in} and C_{eq} are representing the initial and equilibrium copper concentrations (mg/L).

To study the kinetics of the adsorption process, the contact time of the adsorbent with the model solution (20 mg/L) was varied in the range from 15 to 60 minutes. The analysis of the kinetic process parameters was carried out using pseudo-first-order (PFO) and pseudo-second-order (PSO) models, represented by Equation 4 and Equation 5, respectively:

$$ln(a_e - a_t) = lna_e - k_1 t \qquad (4)$$

$$\frac{t}{a_t} = \frac{1}{k_2 a_e^2} + \frac{t}{a_e} \qquad (5)$$

where: a_e and a_t (mg/g) are the adsorption capacity at equilibrium and at any time (min), respectively; k_1 (min⁻¹) and k_2 (g/mg·min) are the PFO and PSO rate constant, respectively.

All adsorption experiments were carried out under static conditions at 20 ± 2 °C and continuous shaking of the samples (Biosan OS-20). The solid-to-liquid phase ratio was 1:500. After the adsorption equilibrium was established, the

liquid phase was separated by centrifugation (3600 rpm), and the equilibrium concentration of copper was determined by inductively coupled plasma atomic emission spectroscopy (Thermo Scientific iCAP 7400 ICP-OES).

The adsorption capacity (a, mg/g) of copper ions was estimated by Equation 6:

$$a = \frac{(C_{in} - C_{eq}) \cdot V}{m} \quad (6)$$

where: C_{in} and C_{eq} represent the initial and equilibrium copper concentrations (mg/L), V is the solution volume (L), and m is the weight of the adsorbent (g).

The Langmuir Equation 7 and Freundlich Equation 8 equations were used to describe the experimental adsorption isotherms of Cu(II) ions:

$$a_e = \frac{a_{max} K_L C_{eq}}{1 + K_L C_{eq}} \quad (7)$$

$$a_e = K_F C_{eq}^{1/n} \quad (8)$$

where: a_e (mg/g) is the equilibrium adsorption capacity, C_{eq} (mg/L) denotes equilibrium concentration, a_{max} (mg/g) is the maximum adsorption capacity, K_L (L/mg) denotes the Langmuir equilibrium constant, and K_F ($(mg/g)(L/mg)^{1/n}$) and 1/n are Freundlich constants related to the adsorption capacity and adsorption intensity, respectively.

RESULTS AND DISCUSSION

The analysis of structural features by IR spectroscopy (Fig. 2) showed that all the vibrational bands characteristic of amorphous silica are present in the studied samples, namely: the vibrational Si-O bond of isolated Si-OH groups (966
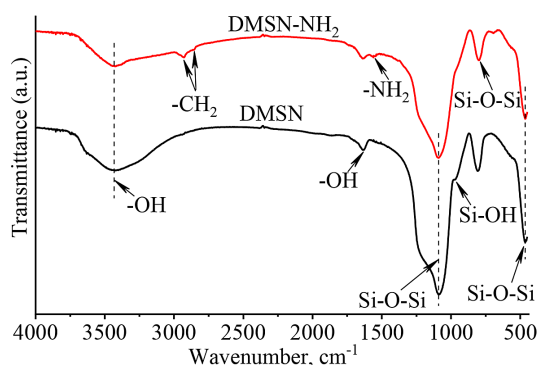

Figure 2. IR spectra of DMSN before and after surface functionalization with amino groups

cm⁻¹), symmetrical valence vibrations (803 cm⁻¹), asymmetrical valence vibrations (1093 cm⁻¹) and bending vibrations (467 cm⁻¹) of the O-Si-O bond (Dong et al., 2023; Li et al., 2021).

The presence of new functional groups (-NH$_2$) was confirmed by the appearance of a shoulder of valence and deformation vibration bands at ~1500 cm⁻¹ (Dhaffouli et al., 2024). In addition, the asymmetric and symmetric stretching modes of -CH$_2$ observed in the range of ~ 2830–2990 cm⁻¹ indicate the presence of APTES propyl chains (Pasternack et al., 2008). The absence of a peak in the ν ~ 3000 cm⁻¹ region, which belongs to the symmetrical stretching of the -N-H bond, may be due to the low intensity of amine groups originating from APTES functionalization (Berktas et al., 2000).

The functionalization of the DMSN surface also transforms the peak in the ν ~ 3400 cm⁻¹ region from the low-frequency side and a shoulder appears in the range of ~ 3200–3000 cm⁻¹. This peak corresponds to the asymmetric vibrations of the -OH group, namely partially hydrated silanols (Si-OH residue) and adsorbed molecular water (Innocenzi et al., 2003; Lei et al., 2009). The peak at 1640 cm⁻¹ characterizes the bending vibrations of the water molecule (Innocenzi et al., 2003).

The content of -OH groups in the initial DMSN sample was 0.16 meq/g. The content of -NH$_2$ groups in the obtained sample, determined as the average of three titration results, was 2.03 meq/g. In the simplest case of functionalization, one hydroxyl group on the DMSN surface reacts with one triethoxysilyl group of APTES (Figure 3).

In this case, the equivalent content of amino groups in the modified sample should be equal to the equivalent content of hydroxyl groups in the initial DMSN. That is, 0.16 meq/g for NH$_2$ groups content. However, the content of amino groups in the resulting sample is significantly higher, which indicates a much more complex mechanism of DMSN modification by APTES. Such a mechanism could, for example, involve partial condensation of APTES with simultaneous functionalization of the DMSN surface (Figure 4).

The number of condensed APTES molecules (n in Figure 4) in the resulting system is likely to vary significantly. Still, the average number n can be calculated by dividing the equivalent content of amino groups by the equivalent content of hydroxyl groups, which is 12.68.

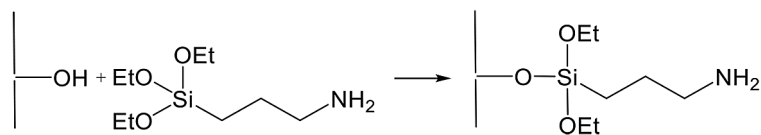Figure 5 shows the DTA and TG curves for the DMSN sample before and after surface

Figure 3. The simplest scheme of interaction of surface -OH groups with APTES
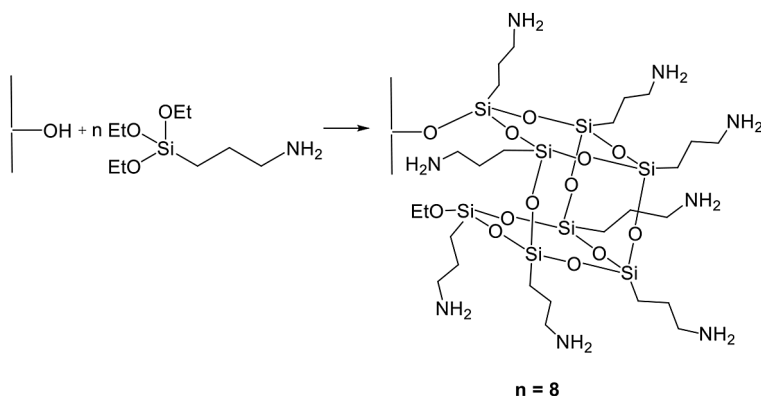

Figure 4. The proposed mechanism of surface functionalization

functionalization. The DTA curves of both samples show similar endo effects at temperatures from 40 to 110 °C, which correspond to the dehydration of the surface of silica particles. In this range, the mass loss (TG curve) is mainly due to the removal of physically bound water, i.e., adsorbed on the surface of the original and modified silica particles (Bergaya et al., 2013; Dugas et al., 2003).

The maximum moisture removal rates differ between the original silica and the modified AP-TES. For the original sample, the maximum corresponds to the endo effect at 69 °C, and for the

modified sample at higher temperatures up to 85 °C. This difference may be due to the influence of amino groups and the possible presence of CO_2 adsorbed from the air, which shifts the maximum moisture removal rate to higher temperatures in the DMSN-NH_2 sample. The period of the second mass loss, between 120–200 °C, is explained by the removal of chemically bound water.

When the temperature exceeds 200 °C, the main contribution to the mass loss is due to the decomposition of organo-functional groups (Sehlleier et al., 2014). According to the literature (Qiao et al., 2015), the boiling point of APTES is 217 °C, so it is assumed that physically adsorbed APTES will be completely removed from the matrix surface by 300 °C. Therefore, the maximum at 280 °C, which is present only in the DMSN-NH_2 sample, probably indicates the cleavage of the amino group in the form of ammonia or oxidation to nitrogen. In general, primary amines are characterized by a large number of possible reactions with the release of gaseous products (Almatarneh et al., 2019).

In the temperature range above 450–500 °C, an exogenous effect is observed when residual alkyl groups that no longer contain nitrogen are oxidized to gaseous products (CO, CO_2). The DTA curve shows that the main decomposition ends by 500 °C. This temperature is consistent with the results of an article (Dugas et al., 2011), which indicates that the C-Si bond begins to break at
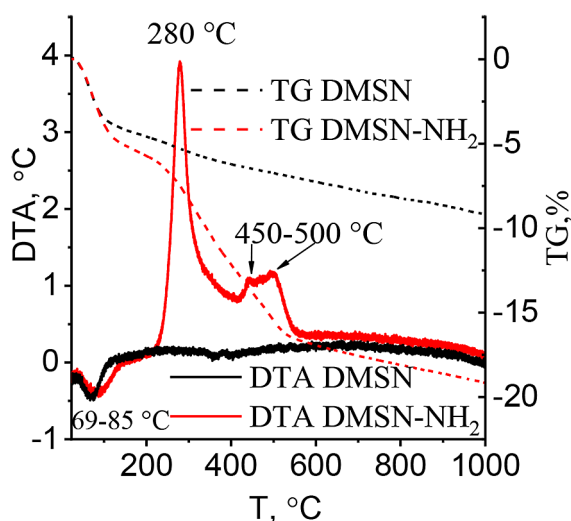

Figure 5. DTA and TG curves for DMSN before and after surface functionalization with amino groups

temperatures of 450–510 °C. The low-temperature nitrogen adsorption/desorption isotherms (Fig. 6a) of both samples under study, according to the IUPAC classification, can be attributed to type IV with H3 hysteresis loops. This type of isotherm is characteristic of materials with a mesoporous structure, which is confirmed by the obtained pore size distribution (Fig. 6b).

The specific surface area of amino-functionalized DMSN (247 m²/g) is lower than that of the original sample (404 m²/g). This decrease is due to the introduction of organic functional groups into the pores, which also reduces their volume. Consequently, the total pore volume decreases from 1.534 cm³/g to 1.073 cm³/g. At the same time, the average pore radius slightly increases from 7.6 nm to 8.7 nm, but before and after functionalization, the local maximum is observed in almost the same range. However, these changes in the pore structure after DMSN functionalization are insignificant. The obtained sample retains 80% of its structural characteristics and can be used as a potential adsorbent for the removal of heavy metal ions from aqueous media.

For the most part, wastewater contaminated with copper ions is acidic. In this case, the predominant form of copper is Cu^{2+}. In addition, at pH 6, the precipitation of $Cu(OH)_2$ from solution begins. Therefore, in this study, the effect of pH on the copper ion removal process was investigated in the range from 3 to 6 (Fig. 7).

The initial DMSN practically does not exhibit adsorption capacity, with a maximum purification efficiency observed at pH 6, reaching only 15%. In contrast, $DMSN-NH_2$ demonstrates highly efficient Cu(II) removal across the entire studied range, with a slight decrease in the degree of purification from 99% to 87% as the pH increases from 3 to 6. The ability of a potential adsorbent to absorb copper ions in an acidic environment is a key factor for the effective removal of Cu(II) from real water bodies, such as concentrated copper-containing wastewater. This is because, in highly concentrated solutions, copper complexes can precipitate at pH values below neutral (Yantasee et al., 2004). Figure 8 shows the time dependence of the Cu(II) adsorption process. In general, the establishment of adsorption equilibrium occurs quite quickly. Within 15 minutes for $DMSN-NH_2$ and 60 minutes for DMSN, the maximum removal of Cu(II) from the model solutions is achieved. Table 1 presents the calculated parameters of the pseudo-first-order and pseudo-second-order kinetic models of this process.

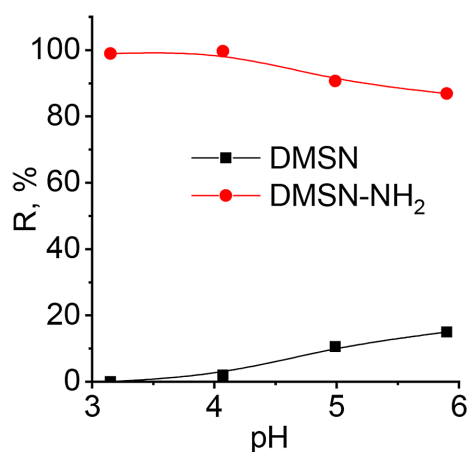The kinetic curves are well described by both models, with $R^2 > 0.99$. This suggests that the

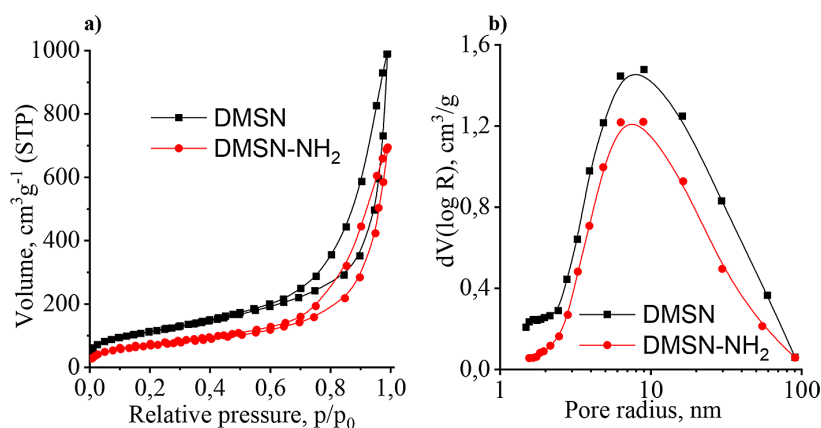**Figure 7.** Dependence of the degree of Cu(II) ion removal on the pH of the aqueous medium by DMSN and $DMSN-NH_2$ samples

Figure 6. Isotherms of low-temperature nitrogen adsorption/desorption (a) and pore size distribution by radius (b) DMSN and $DMSN-NH_2$

Table 1. Coefficients of kinetic equations

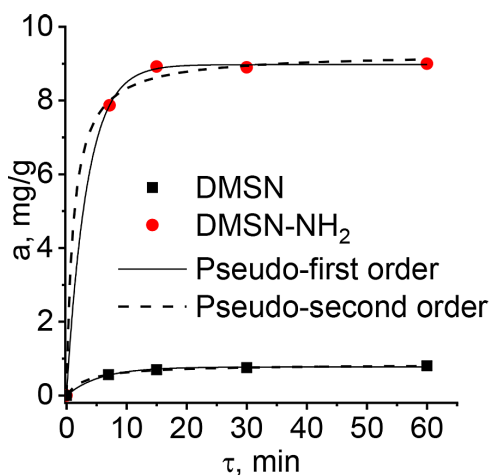| Sample	Pseudo-first-order model			Pseudo-second-order model		
	Qeq, mg/g	k_1, min^{-1}	R^2	Qeq, mg/g	k_2, g/mg·min	R^2
DMSN	0.77	0.17	0.9951	0.84	0.34	0.9992
DMSN-NH$_2$	8.97	0.29	0.9998	9.29	0.09	0.9974

Figure 8. Kinetics of Cu(II) adsorption on the studied samples

adsorption process may occur via a mixed mechanism. At the initial stages, adsorption is rapid due to a high concentration gradient, indicating physical adsorption during the first 10 minutes. As the Cu(II) concentration in the solution decreases, the process rate slows down, and adsorption increasingly involves chemical interactions, such as the formation of complexes or chemical bonds between Cu^{2+} ions and active sites on the material`s surface. However, pseudokinetic models are only general tools for presenting kinetic results. They do not provide a clear physical description of the kinetic mechanism, nor do they determine which adsorption step is more significant (Simonin, 2016). The equilibrium adsorption behavior of Cu^{2+} ions on DMSN and DMSN-NH$_2$ samples, described by the Langmuir and Freundlich adsorption models, is shown in Fig. 9. The results indicate that the adsorption capacity of the synthesized DMSN for copper ions is relatively low, reaching no more

than 0.62 mg/g. For comparison, the adsorption of Cu(II) on commercial SiO$_2$ under similar conditions is 0.3 mg/g (Yu et al., 2023).

When the DMSN surface is modified with amino groups, the adsorption capacity increases by a factor of 50. The calculated parameters of the adsorption equations are summarized in Table 2. The adsorption of Cu(II) on DMSN and DMSN-NH$_2$ samples is well described by both models, further supporting the hypothesis of a mixed adsorption mechanism combining physical adsorption and chemisorption within the studied copper concentration range. To further investigate the mechanism of copper ions adsorption on the surface of amino-functionalized DMSN, XPS analysis of the sample before and after adsorption was performed (Fig. 10). The elemental composition of the initial and treated samples is shown in Table 3. The O1s maximum (about 532 eV), attributed to oxygen and surface hydroxyl groups (Si-OH), represents the main peak of the spectrum. The Si2p and Si2s peaks (about 100–160 eV) correspond to silicon present in the DMSN structure. The C1 peak, at 284 eV is associated with the carbon of the aminopropyl group (-C$_3$H$_6$-NH$_2$), while the N1 peak, at 400 eV corresponds to the nitrogen of the amino group.

The DMSN-NH$_2$*Cu sample, with adsorbed copper ions has a characteristic Cu2p$_{3/2}$ peak at 933.6 eV. Notably, the interaction between Cu^{2+} ions and amino groups leads to an increase in the intensity of the O1 and N1 peaks and their partial shift to the higher energy zone. In order to evaluate the possibility of reusing DMSN-NH$_2$, desorption experiments were conducted to determine its regeneration efficiency over three cycles of copper ion adsorption/desorption.

Table 2. Coefficients of adsorption equations

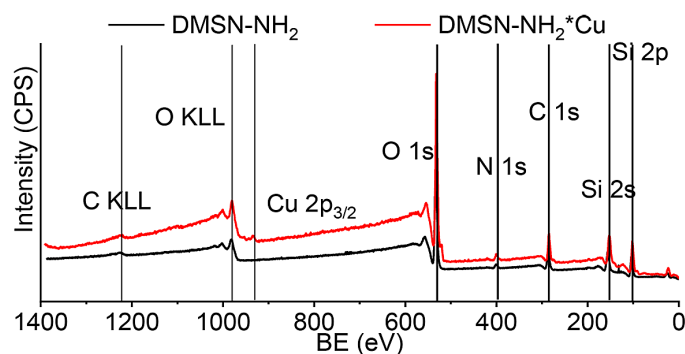| Sample	Langmuir model			Freundlich model		
	Q_{max}	K_L	R^2	K_F	n	R^2
DMSN	0.76	1.16	0.8517	0.56	11.7	0.8387
DMSN-NH$_2$	37.5	0.74	0.9671	17.61	3.9	0.9667

Figure 10. XPS of amino-functionalized DMSN before and after adsorption Cu(II)
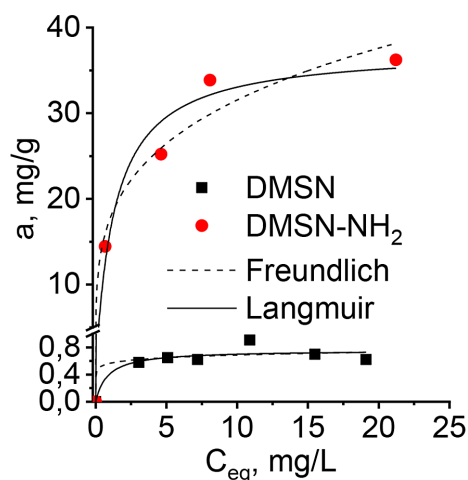
Figure 9. Adsorption isotherms of Cu(II) on DMSN and DMSN-NH$_2$ samples

Table 3. Elemental composition of the samples

Element	Initial	Treated
	Concentration, at.%	Concentration, at.%
C	22.83	18.57
N	2.96	2.28
O	49.47	51.91
Si	24.74	26.83
Cu	-	0.41

adsorption centers, structural changes in DMSN, and modifications in the chemical properties of the -NH$_2$ groups – require further investigation.

The adsorption of copper ions was carried out under the following optimal conditions: the solid-to-liquid phase ratio was 1:500, the interaction duration was 60 min, the concentration of the Cu(II) model solution was 100 mg/L, the ionic strength was 0.01, and the pH was 5.7. Copper ion desorption from the DMSN-NH$_2$ surface was achieved using 0.1 M HCl. Before this, the spent sample was washed several times with distilled water, followed by 60 minutes of stirring in 0.1 M HCl at a solid-to-liquid phase ratio of 1:500. After centrifugation, the copper ion concentration in the liquid phase was determined. The solid phase was then repeatedly washed with distilled water, and a single wash with 0.01 M NaOH solution was performed to activate the amino groups.

Using 0.1 M HCl was found that the desorption capacity after each cycle was 10%, while the adsorption capacity of the material increased by 50%. The underlying reasons for this phenomenon – including the potential activation of novel

CONCLUSIONS

The obtained results confirm the successful synthesis and amino-functionalization of dendritic mesoporous silica nanoparticles (DMSN). It was determined that the content of -NH$_2$ groups in the modified sample is significantly higher than the content of -OH groups in the initial sample – 2.03 meq/g and 0.16 meq/g, respectively. This confirms a complex modification mechanism involving partial condensation of APTES with simultaneous functionalization of the DMSN surface.

At the same time, the textural parameters of the material underwent notable changes, characterized by a decrease in specific surface area from 404 m^2/g to 247 m^2/g and a reduction in total pore volume from 1.534 cm^3/g to 1.073 cm^3/g. Nevertheless, the mesoporous structure remained largely intact. Structural, morphological, and adsorption studies demonstrated that the modification of the DMSN surface with amino groups significantly enhances the efficiency of copper (Cu^{2+}) ion removal from aqueous solutions. DMSN-NH$_2$

exhibited high adsorption capacity (up to 99%) even in acidic environments, as confirmed by kinetic and isothermal adsorption models. The results of XPS analysis indicate the formation of coordination bonds between Cu^{2+} ions and amino groups, suggesting a combination of physical adsorption and chemisorption. Preliminary research on the regeneration and reuse of the material suggests that effective reuse is feasible. However, further research is needed to study the optimal conditions for this process in detail. The DMSN-NH_2 offers several advantages, including a simple synthesis process, control over particle size and texture parameters, and easy separation from the liquid phase. However, the material also has certain drawbacks, such as high dispersion, which may reduce accessibility to active sites. Consequently, the modified DMSN-NH_2 are promising adsorbents for the effective treatment of wastewater contaminated with heavy metal ions.

REFERENCES

1. Vareda, J.P., Valente, A.J.M. & Durães, L. (2019). Assessment of heavy metal pollution from anthropogenic activities and remediation strategies: A review. *Journal of Environmental Management, 246*, 101–118. https://doi.org/10.1016/j.jenvman.2019.05.126

2. Adriano, D.C., Wenzel, W.W., Vangronsveld, J. & Bolan, N.S. (2004). Role of assisted natural remediation in environmental cleanup. *Geoderma*, *122*(2–4), 121–142. https://doi.org/10.1016/j.geoderma.2004.01.003

3. Lejwoda, P., Świnder, H. & Thomas, M. (2023). Evaluation of the mobility of heavy metals in the sediments originating from the post-galvanic wastewater treatment processes. *Environmental Geochemistry and Health*, *45*, 7877–7888. https://doi.org/10.1007/s10653-023-01686-6

4. Izydorczyk, G., Mikula, K., Skrzypczak, D., Moustakas, K., Witek-Krowiak, A. & Chojnacka, K. (2021). Potential environmental pollution from copper metallurgy and methods of management. *Environmental Research*, *197*, 111050. https://doi.org/10.1016/j.envres.2021.11105

5. Mohajerani, A., Vajna, J. & Ellcock, R. (2018). Chromated copper arsenate timber: A review of products, leachate studies and recycling. *Journal of Cleaner Production*, *179*, 292–307. https://doi.org/10.1016/j.jclepro.2018.01.111

6. Husak, V. (2015). Copper and copper-containing pesticides: metabolism, toxicity and oxidative stress. *Journal of Vasyl Stefanyk Precarpathian National University*, *2*(1), 39–51. https://doi.org/10.15330/jpnu.2.1.39-51

7. Shaw, J.L.A., Ernakovich, J.G., Judy, J.D., Farrell, M., Whatmuff, M. & Kirby, J. (2020). Long-term effects of copper exposure to agricultural soil function and microbial community structure at a controlled and experimental field site. *Environmental Pollution*, *263*, 114411. https://doi.org/10.1016/j.envpol.2020.114411

8. Lagerström, M., Ytreberg, E., Wiklund, A.-K.E., & Granhag, L. (2020). Antifouling paints leach copper in excess – study of metal release rates and efficacy along a salinity gradient. *Water Research*, *186*, 116383. https://doi.org/10.1016/j.watres.2020.116383

9. Shrestha, R., Ban, S., Devkota, S., Sharma, S., Joshi, R., Tiwari, A.P. et al. (2021). Technological trends in heavy metals removal from industrial wastewater: A review. *Journal of Environmental Chemical Engineering*, *9*(4), 105688. https://doi.org/10.1016/j.jece.2021.105688

10. Saravanan, A., Senthil Kumar, P., Jeevanantham, S., Karishma, S., Tajsabreen, B., Yaashikaa P.R. et al. (2021). Effective water/wastewater treatment methodologies for toxic pollutants removal: Processes and applications towards sustainable development. *Chemosphere*, *280*, 130595. https://doi.org/10.1016/j.chemosphere.2021.130595

11. Ko, Y.G. (2024). Hybrid method integrating adsorption and chemical precipitation of heavy metal ions on polymeric fiber surfaces for highly efficient water purification. *Chemosphere*, *363*, 142909. https://doi.org/10.1016/j.chemosphere.2024.142909

12. Azimi, A., Azari, A., Rezakazemi, M. & Ansarpour, M. (2017). Removal of Heavy Metals from Industrial Wastewaters: A Review. *ChemBioEng Reviews*, *4*(1), 37–59. https://doi.org/10.1002/cben.201600010

13. Zito, P. & Shipley, H.J. (2015). Inorganic nano-adsorbents for the removal of heavy metals and arsenic: a review. *RSC Advances*, 5, 29885–29907. https://doi.org/10.1039/C5RA02714D

14. Kovalchuk, I., Kornilovych, B., Tobilko, V., Bondarieva, A. & Kholodko, Yu. (2022). Adsorption removal of heavy metal ions from multi-component aqueous system by clay-supported nanoscale zero-valent iron. *Journal of Dispersion Science and Technology*, *45*(1), 68–79. https://doi.org/10.1080/01932691.2022.2127754

15. Hao, M., Liu, Y., Wu, W., Wang, S., Yang, X., Chen, Z. et al. (2023). Advanced porous adsorbents for radionuclides elimination. *EnergyChem*, *5*(4), 100101. https://doi.org/10.1016/j.enchem.2023.100101

16. Rasheed, T., Hassan, A.A., Bilal, M., Hussain, T. & Rizwan, K. (2020). Metal-organic frameworks based adsorbents: A review from removal perspective of various environmental contaminants from

wastewater. *Chemosphere*, *259*, 127369. https://doi.org/10.1016/j.chemosphere.2020.127369

17. Anastopoulos, I., Karamesouti, M., Mitropoulos, A. & Kyzas, G.Z. (2017). A review for coffee adsorbents. *Journal of Molecular Liquids*, *229*, 555–565. https://doi.org/10.1016/j.molliq.2016.12.096

18. Solangi, N.H., Kumar, J., Mazari, S.A., Ahmed, S., Fatima, N. & Mubarak, N.M. (2021). Development of fruit waste derived bio-adsorbents for wastewater treatment: A review. *Journal of Hazardous Materials*, *416*, 125848. https://doi.org/10.1016/j.jhazmat.2021.125848

19. Gil, A., Santamaría, L., Korili, S.A., Vicente, M.A., Barbosa, L.V., de Souza, S.D. et al. (2021). A review of organic-inorganic hybrid clay based adsorbents for contaminants removal: Synthesis, perspectives and applications. *Journal of Environmental Chemical Engineering*, *9*(5), 105808. https://doi.org/10.1016/j.jece.2021.105808

20. Crini, G., Lichtfouse, E., Wilson, L.D. & Morin-Crini, N. (2019). Conventional and non-conventional adsorbents for wastewater treatment. *Environmental Chemistry Letters*, *17*, 195–213. https://doi.org/10.1007/s10311-018-0786-8

21. Hokkanen, S., Bhatnagar, A. & Sillanpää, M. (2016). A review on modification methods to cellulose-based adsorbents to improve adsorption capacity. *Water Research*, *91*, 156–173. https://doi.org/10.1016/j.watres.2016.01.008

22. Uddin, M.K. (2017). A review on the adsorption of heavy metals by clay minerals, with special focus on the past decade. *Chemical Engineering Journal*, *308*, 438–462. https://doi.org/10.1016/j.cej.2016.09.029

23. Zhang, T., Wang, W., Zhao, Y., Bai, H., Wen, T., Kang, S. et al. (2021). Removal of heavy metals and dyes by clay-based adsorbents: From natural clays to 1D and 2D nano-composites. *Chemical Engineering Journal,* *420*(2), 127574. https://doi.org/10.1016/j.cej.2020.127574

24. Kołodyńska, D., Krukowska, J. & Thomas, P. (2017). Comparison of sorption and desorption studies of heavy metal ions from biochar and commercial active carbon. *Chemical Engineering Journal*, *307*, 353–363. https://doi.org/10.1016/j.cej.2016.08.088

25. Nekouei, R.K., Pahlevani, F., Assefi, M., Maroufi, S. & Sahajwalla, V. (2019). Selective isolation of heavy metals from spent electronic waste solution by macroporous ion-exchange resins. *Journal of Hazardous Materials*, *371*, 389–396. https://doi.org/10.1016/j.jhazmat.2019.03.013

26. Tan, L., Liu, Y., Meng, F., Wu, P., Xia, Y. & Tang, Y. (2020). 3D hierarchical defect-rich C@MoS$_2$ nanosheet arrays developed on montmorillonite with enhanced performance in Pb(II) removal. *Environmental Science: Nano*, *7*, 3088–3099. https://doi.org/10.1039/D0EN00542H

27. Wamba, A.G.N., Kofa, G.P., Koungou, S.N., Thue, P.S., Lima, E.C., Reis, G.S. et al. (2018). Grafting of Amine functional group on silicate based material as adsorbent for water purification: A short review. *Journal of Environmental Chemical Engineering*, *6*(2), 3192–3203. https://doi.org/10.1016/j.jece.2018.04.062

28. Kostenko, L.S., Tomashchuk, I.I., Kovalchuk, T.V. & Zaporozhets, O.A. (2019). Bentonites with grafted aminogroups: Synthesis, protolytic properties and assessing Cu(II), Cd(II) and Pb(II) adsorption capacity. *Applied Clay Science*, *172*, 49–56. https://doi.org/10.1016/j.clay.2019.02.009

29. Arce, V.B., Gargarello, R.M., Ortega, F., Romañano, V., Mizrahi, M. et al. (2015). EXAFS and DFT study of the cadmium and lead adsorption on modified silica nanoparticles. *Spectrochimica Acta Part A: Molecular and Biomolecular Spectroscopy*, *151*, 156–163. https://doi.org/10.1016/j.saa.2015.06.093

30. Najafi, M., Yousefi, Y. & Rafati, A.A. (2012). Synthesis, characterization and adsorption studies of several heavy metal ions on amino-functionalized silica nano hollow sphere and silica gel. *Separation and Purification Technology*, *85*, 193–205. https://doi.org/10.1016/j.seppur.2011.10.011

31. Yang, Z., Chen, X., Li, S., Ma, W., Li, Y., He, Z. et al. (2020). Effective removal of Cr(VI) from aqueous solution based on APTES modified nanoporous silicon prepared from kerf loss silicon waste. *Environmental Science and Pollution Research*, *27*, 10899–10909. https://doi.org/10.1007/s11356-019-07427-6

32. Shirendev, N., Bat-Amgalan, M., Kano, N., Kim, H.-J., Gunchin, B., Ganbat, B. et al. (2022). A Natural Zeolite Developed with 3-Aminopropyltriethoxysilane and Adsorption of Cu(II) from Aqueous Media. *Applied Sciences*, *12*(22), 11344. https://doi.org/10.3390/app122211344

33. Xu, C., Lei, C., Wang, Y. & Yu, C. (2022). Dendritic Mesoporous Nanoparticles: Structure, Synthesis and Properties. *Angewandte Chemie International Edition*, *61*(12), e202112752. https://doi.org/10.1002/anie.202112752

34. Cabañas, M.V., Lozano, D., Torres-Pardo, A., Sobrino, C., González-Calbet, J., Arcos, D. et al. (2018). Features of aminopropyl modified mesoporous silica nanoparticles. Implications on the active targeting capability. *Materials Chemistry and Physics*, *220*, 260–269. https://doi.org/10.1016/j.matchemphys.2018.09.005

35. Estevão, B.M., Miletto, I., Hioka, N., Marchese, L. & Gianotti, E. (2021). Mesoporous silica nanoparticles functionalized with amino groups for biomedical applications. *ChemistryOpen*, *10*(12), 1251-1259. https://doi.org/10.1002/open.202100227

36. Marconi, E., Luisetto, I., Carlo, G., Staccioli, M.P.,

Tuti, S. & Tortora, L. (2023). 3-APTES on dendritic fibrous mesoporous silica nanoparticles for the pH-controlled release of corrosion inhibitors. *Nanomaterials*, *13*(18), 2543. https://doi.org/10.3390/nano13182543

37. Otalvaro, J.O., Avena, M. & Brigante, M. (2019). Adsorption of organic pollutants by amine functionalized mesoporous silica in aqueous solution. Effects of pH, ionic strength and some consequences of APTES stability. *Journal of Environmental Chemical Engineering*, *7*(5), 103325. https://doi.org/10.1016/j.jece.2019.103325

38. Dhaffouli, A., Salazar-Carballo, P.A., Carinelli, S., Holzinger, M. & Barhoumi, H. (2024). Improved electrochemical sensor using functionalized silica nanoparticles (SiO$_2$-APTES) for high selectivity detection of lead ions. *Materials Chemistry and Physics*, *318*, 129253. https://doi.org/10.1016/j.matchemphys.2024.129253

39. Ramasamy, D.L., Wojtuś, A., Repo, E., Kalliola, S., Srivastava, V. & Sillanpää, M. (2017). Ligand immobilized novel hybrid adsorbents for rare earth elements (REE) removal from waste water: Assessing the feasibility of using APTES functionalized silica in the hybridization process with chitosan. *Chemical Engineering Journal*, *330*, 1370–1379. https://doi.org/10.1016/j.cej.2017.08.098

40. Kuśmierek, K., Świątkowski, A., Zienkiewicz-Strzałka, M. & Deryło-Marczewska, A. (2025). Studies of the kinetics and isotherms of copper ions adsorption on APTES-modified silica materials. *Desalination and Water Treatment*, *321*, 100965. https://doi.org/10.1016/j.dwt.2024.100965

41. Yu, J., Bondarieva, A.I. & Tobilko, V. Yu. (2024). Effect of synthesis time on the morphology of monodisperse silica microspheres. *Journal of Chemistry and Technologies*, *32*(4), 932–938. https://doi.org/10.15421/jchemtech.v32i4.315165

42. Tobilko, V., Spasonova, L., Kovalchuk, I., Kornilovych, B. & Kholodko, Yu. (2019). Adsorption of Uranium (VI) from Aqueous Solutions by Amino-functionalized Clay Minerals. *Colloids and Interfaces*, *3*(1), 41. https://doi.org/10.3390/colloids3010041

43. Tanabe, K., Misono, M., Hattori, H., & Ono, Y. (1990). *New solid acids and bases: their catalytic properties*. Elsevier, 300.

44. Moaseri, E., Baniadam, M., Maghrebi, M. & Karimi, M. (2013). A simple recoverable titration method for quantitative characterization of amine-functionalized carbon nanotubes. *Chemical Physics Letters*, *555*, 164–167. https://doi.org/10.1016/j.cplett.2012.10.064

45. Dong, K., Wu, S., Chang, B. & Sun, T. (2023). Zero-valent iron supported by dendritic mesoporous silica nanoparticles to purify dye wastewater. *Journal of Environmental Chemical Engineering*, *11*(5), 110434. https://doi.org/10.1016/j.jece.2023.110434

46. Li, H., Si, R., Wang, W., Huang, Y., Xiang, M., Wang, C. et al. (2021). Sulfidated nanoscale zero-valent iron dispersed in dendritic mesoporous silica nanospheres for degrading tetrabromobisphenol A. *Colloids and Surfaces A: Physicochemical and Engineering Aspects*, *621*, 126586. https://doi.org/10.1016/j.colsurfa.2021.126586

47. Pasternack, R.M., Amy, S.R. & Chabal, Y.J. (2008). Attachment of 3-(Aminopropyl)triethoxysilane on silicon oxide surfaces: dependence on solution temperature. *Langmuir*, *24*(22), 12963–12971. https://doi.org/10.1021/la8024827

48. Berktas, I., Ghafar, A.N., Fontana, P., Caputcu, A., Menceloglu, Y. & Okan, B.S. Facile synthesis of graphene from waste tire/silica hybrid additives and optimization study for the fabrication of thermally enhanced cement grouts. *Molecules*, *25*(4), 886. https://doi.org/10.3390/molecules25040886

49. Innocenzi, P., Falcaro, P., Grosso, D. & Babonneau, F. (2003). Order-disorder transitions and evolution of silica structure in self-assembled mesostructured silica films studied through FTIR spectroscopy. *The Journal of Physical Chemistry B*, *107*(20), 4711–4717. https://doi.org/10.1021/jp026609z

50. Lei, Z., Pang, X., Li, Na, Lin, L. & Li, Y. (2009). A novel two-step modifying process for preparation of chitosan-coated Fe$_3$O$_4$/SiO$_2$ microspheres. *Journal of Materials Processing Technology*, *209*(7), 3218–3225. https://doi.org/10.1016/j.jmatprotec.2008.07.044

51. Bergaya, F. & Lagaly, G. (2013). *Handbook of Clay Science. Second Edition*. Elsevier, 814.

52. Dugas, V. & Chevalier, Y. (2003). Surface hydroxylation and silane grafting on fumed and thermal silica. *Journal of Colloid and Interface Science*, *264*(2), 354–361. https://doi.org/10.1016/S0021-9797(03)00552-6

53. Sehlleier, Y.H., Abdali, A., Schnurre, S.M., Wiggers, H. & Schulz, C. (2014). Surface functionalization of microwave plasma-synthesized silica nanoparticles for enhancing the stability of dispersions. *Journal of Nanoparticle Research*, *16*, 2557. https://doi.org/10.1007/s11051-014-2557-1

54. Qiao, B., Wang, T.-J., Gao. H. & Jin, Y. (2015). High density silanization of nano-silica particles using γ-aminopropyltriethoxysilane (APTES). *Applied Surface Science*, *351*, 646–654. https://doi.org/10.1016/j.apsusc.2015.05.174

55. Almatarneh, M.H., Elayan, I.A., Al-Sulaibi, M., Khawaldeh, A.A., Saber, S.O.W., Al-Qaralleh, M. et al. (2019). Unimolecular decomposition reactions of propylamine and protonated propylamine. *ACS Omega*, *4*(2), 3306–3313. https://doi.org/10.1021/acsomega.8b02792

56. Dugas, V. & Chevalier, Y. (2011). Chemical reactions

in dense monolayers: in situ thermal cleavage of grafted esters for preparation of solid surfaces functionalized with carboxylic acids. *Langmuir*, *27*(23), 14188–14200. https://doi.org/10.1021/la2029438

57. Yantasee, W., Lin, Y., Fryxell, G.E., Alford, K.L., Busche, B.J., & Johnson, C.D. (2004). Selective removal of copper(II) from aqueous solutions using fine-grained activated carbon functionalized with amine. *Industrial & Engineering Chemistry Research*, *43*(11), 2759–2764. https://doi.org/10.1021/ie030182g

58. Simonin, J.-P. (2016). On the comparison of pseudo-first order and pseudo-second order rate laws in the modeling of adsorption kinetics. *Chemical Engineering Journal*, *300*, 254–263. https://doi.org/10.1016/j.cej.2016.04.079

59. Yu, J., Bondarieva, A., Tobilko, V., Pavlenko, V. (2023). Adsorption removal of Cu (II) using Ni-modified silica gel. *Water and Water Purification Technologies. Scientific and Technical News*, *37*(3), 3–12. https://doi.org/10.20535/2218-930032023302423